ACCOUNTS of chemical research

Article

pubs.acs.org/accounts

Visualization of Colloidal Nanocrystal Formation and Electrode−Electrolyte Interfaces in Liquids Using TEM

Published as part of the Accounts of Chemical Research special issue "Direct Visualization of Chemical and Self-Assembly Processes with Transmission Electron Microscopy".

Zhiyuan Zeng,[†] Wenjing Zheng,[†,‡] and Haimei Zheng*[,†,§]

[†]Materials Sciences Division, Lawrence Berkeley National Laboratory, Berkeley, California 94720, United States

[‡]Department of Materials Science and Engineering, Tianjin University, Tianjin 300350, China

[§]Department of Materials Science and Engineering, University of California, Berkeley, California 94720, United States

CONSPECTUS: Transmission electron microscopy (TEM) has become a powerful analytical tool for addressing unique scientific problems in chemical sciences as well as in materials sciences and other disciplines. There has been a lot of recent interest in the development and applications of liquid phase environmental TEM. In this Account, we review the development and applications of liquid cell TEM for the study of dynamic phenomena at liquid−solid interfaces, focusing on two areas: (1) nucleation, growth, and self-assembly of colloidal nanocrystals and (2) electrode−electrolyte interfaces during charge and discharge processes. We highlight the achievements and progress that have been made in these two topical areas of our studies. For example, tracking single platinum particle growth trajectories revealed that two different pathways of growth, either by monomer attachment or coalescence between nanoparticles, led to the same particle size. With the improved spatial resolution and fast electron detection, we were able to trace individual facet development during platinum nanocube platinum nanocube growth. The results showed that different from the surface energy minimization rule prediction, the growth rates of all low-energy facets, such as {100}, {110}, and {111}, were similar. The {100} facets stopped growth early, and the continuous growth of the rest facets resulted in a nanocube. Density functional theory calculations showed that the amine ligands with low mobility on the {100} facets blocked the further growth of the facets. The effect of the ligand on nanoparticle shape evolution were further studied systematically using a Pt−Fe nanoparticle system by changing the oleylamine concentration. With 20%, 30%, or 50% oleylamine, Pt−Fe nanowires or nanoparticles with different morphologies and stabilities were achieved. Real-time imaging of nanoparticles in solution also enabled the study of interactions between nanoparticles during self-assembly. We further compared the study of noble-metal nanoparticles and transition-metal oxides in a liquid cell to elucidate the nanoparticle formation mechanisms. In the second part of this Account, we review the study of electrolyte−electrode interfaces by the development of electrochemical liquid cell TEM. The formation of single-crystalline Pb dendrites from polycrystalline branches and Li dendrite growth in a commercial electrolyte for Li ion batteries were observed. We also studied lithiation reactions of MoS_2 and Au electrodes. MoS_2 nanoflakes on the Ti electrode underwent irreversible decomposition, resulting in the vanishing of the MoS_2 active nanoflakes. More detailed study using nanobeam diffraction indicated that the MoS_2 nanoflakes were broken down into small nanoparticles as a result of the fast discharge. For the lithiation of Au electrodes, three distinct types of morphology changes during reactions were revealed, including gradual dissolution, explosive reaction, and local expansion/shrinkage. Additionally, we studied electrolyte decomposition reactions such as bubble formation and solid electrolyte interphase formation. At the end, our perspective on the challenges and opportunities in the applications of liquid phase environmental TEM for the study of liquid chemical reactions is provided.

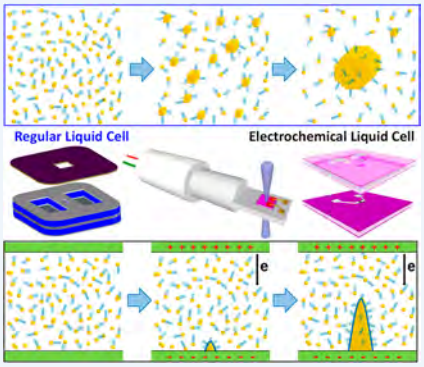

1. INTRODUCTION

Transmission electron microscopy (TEM) has been extensively used in high-resolution characterization of materials in materials science, physics, and chemistry. TEM has also been an indispensable tool in imaging of fine biological structures at cryogenic temperature.[1] In recent years, it has become more and more popular to use TEM to study chemical reactions in liquids[2−4] or gases[5] in situ; significant advances have been made in the development and applications of liquid phase environment TEM.[3,6,7] In this Account, we review the progress in imaging through liquids with TEM, highlighting some of our work in the past a few years on TEM visualization of colloidal nanocrystal growth and electrochemical reactions in liquids (Figure 1).

Received: April 3, 2017
Published: August 7, 2017

DOI: 10.1021/acs.accounts.7b00161
Acc. Chem. Res. 2017, 50, 1808−1817

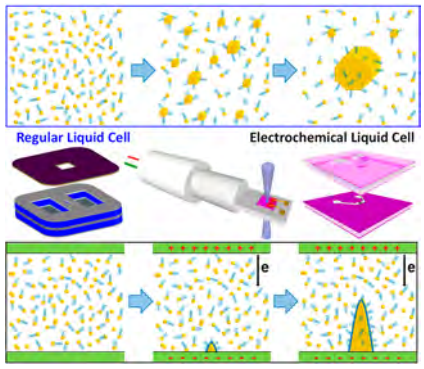

Figure 1. Schematic overview of TEM visualization of colloidal nanocrystal growth and electrochemical liquid reactions.

The study of liquid-phase reactions and an understanding of solid–liquid interfaces are significant for various applications ranging from solution-based synthesis to energy conversion and fuel generation, catalysis, materials corrosion protection, and water separation. Atomic- or molecular-level imaging and spectroscopy of solid-liquid interfaces has attracted a lot of recent attention. Characterization of liquid samples using TEM is challenging because the samples are incompatible with the high-vacuum environment needed for electron microscopy. Hence, the development of liquid cells allowing for imaging through liquids with TEM has attracted lots of attention in recent years. With nanofabricated liquid cells using revolutionary thin SiN_x window cells and integrated electrodes, we have been able to address some scientific problems concerning solid-liquid interfaces with high spatial and temporal resolution that are previously inaccessible. Liquid phase environmental TEM has attracted broad interest. It has been applied to the study of nanoparticle growth and assembly in solution, electrochemical deposition, lithiation of electrode materials in batteries, tracing or manipulating nanoparticles, catalysis, imaging of biological materials in liquid water and so on.[1,8−11]

2. NUCLEATION AND GROWTH OF COLLOIDAL NANOCRYSTALS

2.1. Growth Pathways

An understanding of colloidal nanocrystal growth mechanisms is significant for the syntheses of nanocrystals with desired physical and chemical properties. Many growth models for achieving monodisperse nanocrystals are built upon nucleation followed by growth via monomer attachment.[12] However, there have been numerous reports showing that monodisperse nanocrystals can be achieved by nanoparticle coalescence, where a bigger nanoparticle can be achieved by different nanoparticles being agglomerated together,[13−15] or via oriented attachment[1] that nanoparticles attached together with the aligned crystal orientation. Intuitively, growth via nanoparticle coalescence or agglomeration is uncontrollably fast resulting in polydispersity, thus particle coalescence should be avoided. The ability to observe single-nanoparticle growth trajectories provides the opportunity to elucidate nanocrystal growth mechanisms, and TEM liquid cells were the key development allowing imaging through liquids with nanometer or atomic resolution in real time while reactions proceed.

Zheng et al.[2] developed ultrathin self-contained liquid cells and first applied them to study colloidal platinum nanocrystals by solution chemistry using TEM. As shown in Figure 2,

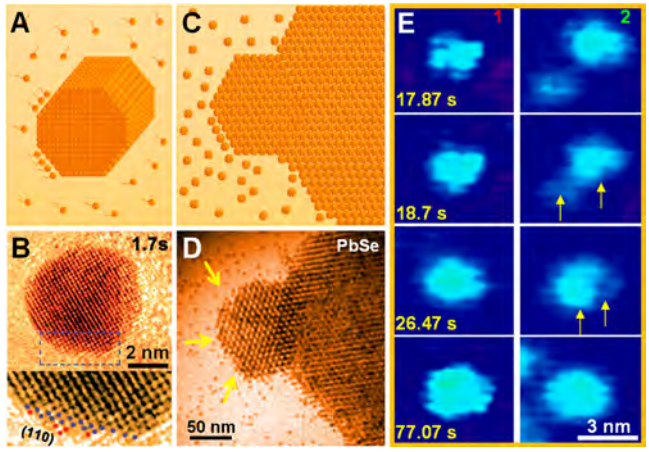

Figure 2. (A) Schematic showing the atomic growth of a nanoparticle. (B) Atomic growth of the (110) facet of a platinum nanoparticle. The red dots show the newly added Pt atoms. Reprinted with permission from ref 21. Copyright 2014 American Association for the Advancement of Science. (C) Schematic showing the self-assembly of nanoparticles. (D) Observed self-assembly of PbSe nanoparticles in a liquid cell. (E) Comparison of different growth trajectories of platinum nanoparticles. Enlarged (1.5 times) color images from an in situ movie showing simple growth by monomer addition (left column) or growth by coalescence between nanoparticles (right column) are presented. Distinct contrast changes are highlighted with arrows indicating recrystallization within the particle after coalescence. Reprinted with permission from ref 2. Copyright 2009 American Association for the Advancement of Science.

observations revealed that monodisperse nanocrystals can be achieved by nanoparticles growing simultaneously via different pathways: atomic attachment and particle coalescence. Real-time imaging further indicated that particles formed by simple monomer attachment show a continuous increase in particle size with single-crystalline characteristics throughout the growth. The coalesced particle is polycrystalline at the beginning. It subsequently undergoes shape changes and finally forms a single-crystalline particle. During such a restructuring process, the growth by monomer attachment slows down. Thus, two different growth pathways lead to the same particle size (Figure 2E). Through the combination of these two routes, an initially broad size distribution can spontaneously narrow down into a nearly monodisperse distribution. There are important questions concerning nanoparticle growth by coalescence. For example, how do nanoparticles interact with each other? What are the forces between nanoparticles? The answers to these questions are important for nanoparticle synthesis as well as the self-assembly of nanoparticles into thin films or other three-dimensional structures. Previous studies showed that colloidal nanocrystals take different pathways of growth driven by their size- and morphology-dependent internal energy, and details have been reported in publications.[2,16,17]

2.2. Nanoparticle Shape Evolution

Liquid phase environmental TEM has been used to reveal the shape evolution of nanoparticles, where formation mechanisms of nanocubes, nanorods, plates, etc. can be resolved. A liquid cell with a small amount of liquid can be encapsulated inside a high-vacuum microscope for an extended period of time. It allows nanoparticles to nucleate and fully develop into different shapes. Nanocrystal nucleation and growth can be initiated by thermal heating[18] or, more commonly, by electron beam

DOI: 10.1021/acs.accounts.7b00161
Acc. Chem. Res. 2017, 50, 1808−1817

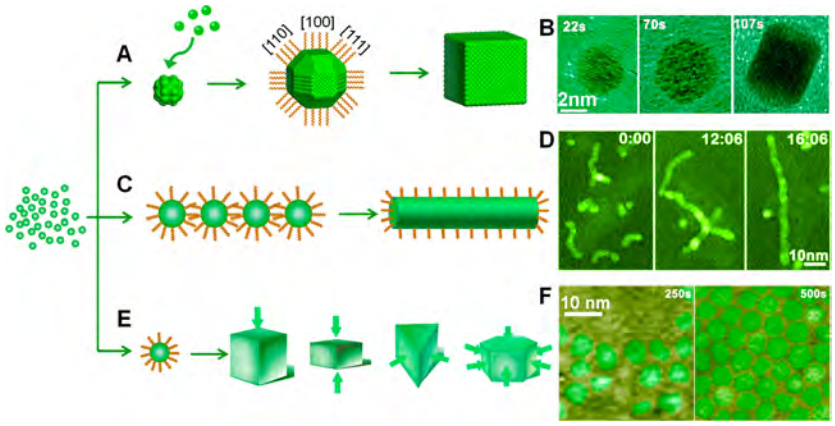

Figure 3. (A) Schematic illustrating the growth of a nanocube in a liquid solution. (B) Sequential images showing the growth of a Pt nanocube. Reprinted with permission from ref 21. Copyright 2014 American Association for the Advancement of Science. (C) Schematic showing nanowire formation by shape-directed nanoparticle attachment. (D) Sequential TEM images showing the growth of a Pt_3Fe nanorod. Time is displayed as minutes:seconds. The initial time is arbitrary. Nanorods and the specific particles as building blocks for nanorod formation are highlighted in green. Reprinted with permission from ref 16. Copyright 2012 American Association for the Advancement of Science. (E) Schematic demonstrating stereohindrance effects during growth. (F) Sequential images indicating the growth of platinum−iron nanocrystals in a solvent with 50% oleylamine. Nanoparticles are highlighted in green. Reprinted from ref 25. Copyright 2013 American Chemical Society.

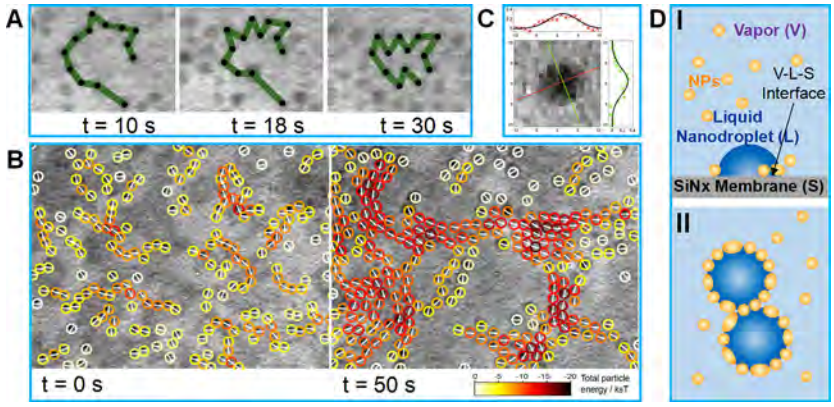

Figure 4. (A) Dynamics of nanoparticles aligned in one-dimensional chains. Chains formed at the beginning of assembly have a particle connectivity that is tracked over time to illustrate folding and clumping behavior. Reprinted from ref 17. Copyright 2016 American Chemical Society. (B) Energy and stability of self-assembly. Colored circles indicate locations of nanoparticles overlaid on the original image. White arrows indicate dipole orientations. The colors correspond to the total energies of individual nanoparticles computed from the dipole and van der Waals interactions with nearby particles. Reprinted from ref 17. Copyright 2016 American Chemical Society. (C) Identification of a nanoparticle by image processing. (D) A schematic showing nanoparticles assembled around a liquid nanodroplet.

irradiation.[9] Despite many unknown factors in electron-beam-activated reactions, nanocrystals similar to those in flask synthesis have been achieved in a liquid cell.[19−21]

The Zheng group reported in situ liquid cell TEM imaging of platinum nanocube growth with high spatial and temporal resolution (Figure 3A,B).[21] Tracking of individual facet evolution showed that the growth rates of all low-index facets, e.g., {100}, {110}, and {111}, are similar until the {100} facets stop growing. The continuous growth of the rest facets leads to a nanocube. Calculations indicated that the arrest of {100} facet growth can be attributed to the lower ligand mobility on the {100} facets. At the end, only the {111} facets grow, filling the corners until the nanoparticle becomes a cube. This study provided critical insights into the role of ligands in controlling nanocrystal shape evolution. It was also concluded that at the nanoscale the stochastic nature dominates the nanocrystal growth, which is different from the Wulff construction prediction that the higher-energy facets grow faster and the nanocrystal morphology is determined by the relative surface energies of the different crystalline facets.[12,22]

Many recent studies have shown that nanoparticles can act as "artificial atoms" to serve as the basic building blocks for the synthesis of hierarchical nanostructures.[12,22] As discussed in the previous section, small nanoparticles interact with each other to form a large single crystal through oriented attachment.[23,24] Liao et al.[16] reported the solution growth of Pt_3Fe nanorods, where a nanoparticle chain was achieved by shape-directed nanoparticle attachment, and the subsequent straightening of the chain with crystal orientation correction resulted in a single-crystal nanorod. Tracking the nanoparticle growth trajectories assisted in differentiating the forces exerted by a single nanoparticle or a nanoparticle chain (Figure 3C,D).

A systematic study of ligand effects on nanoparticle formation was further carried out (Figure 3E,F).[25] When the oleylamine concentration was changed from 30% to 20%, nanoparticles were still able to end-to-end attach together to form a nanowire. However, the nanowire subsequently broke

DOI: 10.1021/acs.accounts.7b00161
Acc. Chem. Res. 2017, 50, 1808−1817

down into pieces, and each piece shrank into a round particle. A large size distribution of the nanoparticles was observed. With a higher concentration of oleylamine, such as 50% or more, the individual nanoparticles were stablized in solution.

Interactions between nanoparticles can be complex, and a variety of forces may be involved, such as van der Waals forces, electric or magnetic dipolar forces, liquid surface tension in drying-mediated self-assembly, etc.[24,26,27] Powers et al.[17] observed and quantified the complex dynamics of Pt−Fe nanoparticle self-assembly directly. The long-range anisotropic electric dipolar forces and the close-range van der Waals interactions result in the formation of loosely packed clumps.[17] The chains fold to form either locally packed clumps or a two-dimensional film (Figure 4A). The results prove that the long-range forces and particle interactions observed for $PtFe_3$ are inherent to the particle properties (Figure 4B). Nanoparticles can be assembled around a liquid droplet and ring-like deposits along the perimeter of liquid droplet can be found. The mechanism behind the formation of these and similar rings is known as the coffee ring effect (Figure 4D).

2.3. Metal versus Oxide Nanoparticle Growth

Transition-metal oxides, such as spinel ferrites MFe_2O_4 with M(II) corresponding to Fe^{2+}, Mn^{2+}, Ni^{2+}, Zn^{2+}, or Cu^{2+}, have many applications ranging from biomedicine[28] to catalysis[29] and high-density magnetic storage.[30] An understanding of their formation mechanisms and ultimately control of the synthesis have been of great interest. There have been many studies on in situ observation of noble-metal nanocrystal formation using liquid cell TEM to elucidate the electron-beam-induced growth mechanisms.[31,32] However, there are a limited number of reports on the formation of metal oxide nanoparticles in a liquid cell.

Liang and co-workers reported the study of M−Fe oxide (M = Ni, Mn, Co, Zn) nanoparticles using liquid cell TEM.[33,34] A growth solution of metal acetylacetonates dissolved in oleylamine, oleic acid, and benzyl ether was used. Nickel iron oxide or cobalt iron oxide nanocrystals with spinel structure were obtained under electron beam irradiation of the Ni−Fe or Co−Fe precursor solution (Figure 5A). The study also showed that with the solution containing Mn−Fe or Zn−Fe precursor, iron oxide nanoparticles were achieved with Mn or Zn remaining in the solution (Figure 5B). Ternary oxides (i.e., Ni−Fe oxide and Co−Fe oxide) were achieved when the two precursors have smaller difference in metal ion reduction potentials ΔE_r and thermal decomposition temperature ΔT_d, such as Ni−Fe and Co−Fe mixed precursor solution, whereas the single-metal-component oxide with lower decomposition temperature (T_d) and stronger reduction potential (E_r) (i.e., Fe oxide) was obtained, for example, from a Mn−Fe or Zn−Fe mixed precursor solution.[33] These results shed light on synthetic strategies for incorporating multiple components in the oxide nanostructures.

In another study using an Fe−Pt precursor solution, Liang et al.[34] obtained transition-metal oxide core−shell nanostructures (Figure 5C−E). Detailed characterization using energy-dispersive X-ray spectroscopy (EDS) elemental mapping, electron energy loss spectroscopy (EELS), and high-resolution structure analysis confirmed the Fe_3Pt−Fe_2O_3 core−shell structure. A formation mechanism for Fe_3Pt−Fe_2O_3 core−shell nanoparticles was proposed as shown in Figure 5E. Briefly, Pt ions are reduced to Pt metal under the electron beam as a result of the higher redox potential as well as the lower

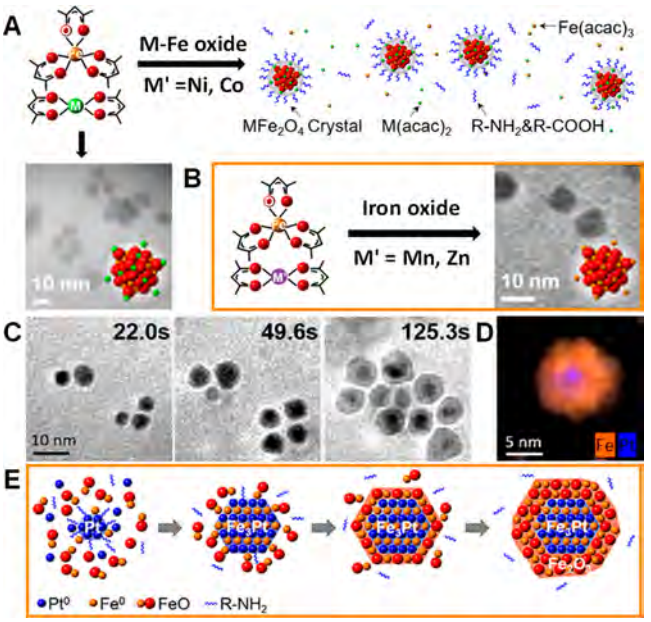

Figure 5. (A) Illustration of spinel ferrite M−Fe oxide growth in liquid cell TEM. (B) Illustration of Fe oxide growth in a liquid cell. (C) Sequential images captured during growth of Fe_3Pt−Fe_2O_3 core−shell nanostructures. (D) EDS mapping of one core−shell nanoparticle. Blue represents Pt, and orange represents Fe. (E) Schematic summarizing the formation pathway of the Fe_3Pt−Fe_2O_3 core−shell heterostructure. Reprinted from (A, B) ref 33 and (C−E) ref 34. Copyright 2015 American Chemical Society.

decomposition temperature of $Pt(acac)_2$ compared with $Fe(acac)_3$.[35] Once Pt^0 is formed, oleylamine ligands ($R-NH_2$) prefer to bind with Pt (stage I).[36] Thus, Fe^{3+} ions can be reduced to form Fe_3Pt, where Pt catalyzes the electron transfer between oleylamine and Fe ions.[35] When Pt is depleted in the precursor solution, the nanoparticle core size is fixed, and the Fe ions adsorbed on the nanoparticle surface develop into iron oxide without further reduction. Most of the nanoparticles show a polycrystalline shell, likely due to the large lattice mismatch between Fe_3Pt and α-Fe_2O_3.[34]

It is noted that besides nanoparticle growth, etching of nanoparticles has also been observed in liquid cells[37,38] Schneider et al.[38] and others[39−41] showed that the electron beam plays an important role in crystallization as well as etching. Thus, quantitative studies of the effects of the electron beam are necessary to elucidate the growth mechanisms observed in a liquid cell under TEM.

3. CRYSTALLIZATION AND REACTIONS UNDER ELECTROCHEMICAL BIAS

3.1. Dendritic Growth

Dendritic growth has attracted a large amount of research interest in recent years.[42−46] It is ubiquitous in materials solidification and crystallization and arises from instabilities when the growth rate is limited by the diffusion of ions from solution to the deposits. Dendrite formation can induce device failure—for example, a dendrite may connect two electrodes of a battery cell. Real-time observation of the electrochemical growth with high spatial resolution provides the opportunity to elucidate the dendrite growth mechanisms and insights on new strategies to reduce battery failure.[7,8,47,48]

DOI: 10.1021/acs.accounts.7b00161
Acc. Chem. Res. 2017, 50, 1808−1817

Sun et al.[49] reported in situ TEM imaging of the deposition and dissolution of lead dendrites on the electrodes during discharge−charge processes. Unique crystallization pathways were revealed. As shown in Figure 6A,B, Pb ions were first reduced to form small grains on the electrode. Subsequently, those grains aggregated to form a large cluster with polycrystalline features. Eventually, a single-crystalline structure was achieved through interactions between nanograins and recrystallization.

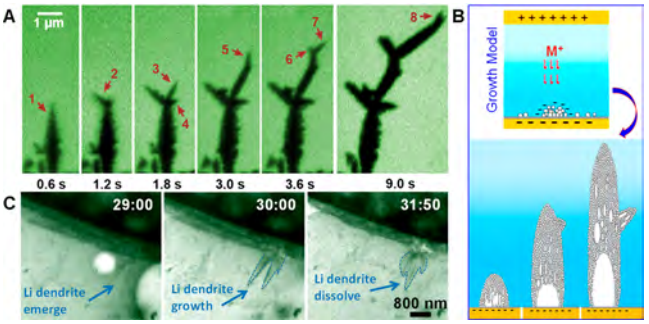

Figure 6. (A) Time series of TEM images and (B) a schematic showing the electrochemical growth of lead dendrites. Reprinted with permission from ref 49. Copyright 2013, rights managed by Nature Publishing Group. (C) Time evolution of the growth and dissolution of a lithium dendrite. Adapted from ref 48. Copyright 2014 American Chemical Society.

Using a commercial electrolyte for lithium ion batteries, we have also observed lithium dendrite growth in situ. As shown in Figure 6C, the lithium dendrite nucleates between two bubbles and grows rapidly on the Au alloy layer (highlighted by blue arrows). The lithium dendrite preserves its shape for a short time; when the voltage is swept back, localized Li stripping occurs, and thus, the dendrite eventually dissolves.

There have been other reports on in situ observation of electrodeposition related to dendrite formation. For example, Radisic et al.[47] reported imaging of electrochemical deposition of polycrystalline Au using an electrochemical liquid cell. Chen et al.[50] achieved deposition of nickel nanograins with a homemade TEM cell. White et al.[51] captured electrodeposition and stripping of lead on polycrystalline gold electrodes.

3.2. Electrode Reactions: MoS_2 Dissolution and Au Lithiation Reactions

We recently observed lithiation/delithiation of MoS_2 nanosheets in a $LiPF_6$/EC/DEC commercial electrolyte.[52] There have been a series of related studies on lithiation- and delithiation-induced structural transformations using in situ TEM.[52−55] For instance, lithiation and delithiation of Si nanowire electrodes during electrochemical testing[53] showed that the first lithiation of Si nanoparticles leads to anisotropic volume expansion favoring the ⟨110⟩ directions followed by isotropic expansion.[56] There have also been studies on atomic imaging of lithium insertion and extraction dynamics in partially delithiated $LiFePO_4$[57] and the random solid-solution zone in $LiFePO_4$ electrodes[58] and the breakdown of a range of inorganic/salt complexes in Li-ion batteries.[55]

Our observation of lithiation/delithiation of MoS_2 nanosheets showed that MoS_2 on the Ti electrode underwent irreversible decomposition resulting in fast dissolution and vanishing of MoS_2 nanoflakes (Figure 7A), which is consistent with other literature reporting on electrode material dissolution and the lithium polysulfide shuttling effects in a real battery cell.[59] Repeated experiments also indicate lithiation-induced structural expansion and deformation of MoS_2 nanosheets. In addition, fast discharge induces "explosion" of some MoS_2 nanosheets into 5−10 nm MoS_2 nanoparticles.[4,52]

It has been a serious issue that mechanical stress can be generated during lithiation and delithiation processes, which induces pulverization with rapid capacity fading. Although

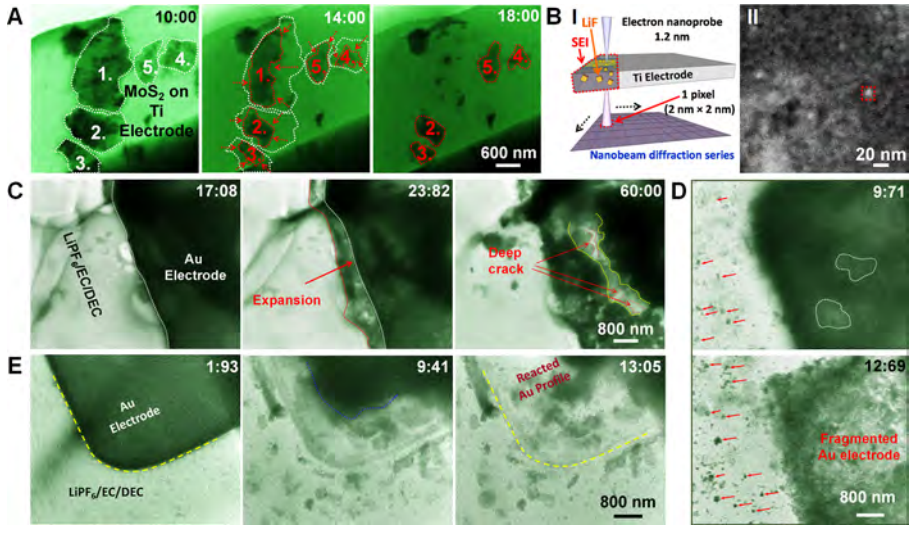

Figure 7. (A) Time series of TEM images showing the morphological evolution of MoS_2 nanosheets on the Ti electrode with $LiPF_6$/EC/DEC electrolyte in a liquid cell. (B) I. Schematic showing nanobeam diffraction characterization of the SEI layer or residual MoS_2 products after the reaction. II. Long camera length (770 mm) STEM image with nanobeam diffraction series acquired in the area marked with the red dashed box. (C) Evolution of a Au electrode when electrochemically reacted with lithium electrolyte. Expansion and cracking are observed. (D) Time series of TEM images showing the fragmentation of a Au electrode during Li−Au reaction. During this explosive reaction, a large number of nanoparticles splashed from the Au electrode to the surrounding area of the electrode. (E) Time evolution of the dissolution of a Au electrode in $LiPF_6$/EC/DEC electrolyte. (A, B) Adapted from ref 52. Copyright 2015 American Chemical Society. (C−E) Adapted with permission from ref 64. Copyright 2014 Royal Society of Chemistry.

DOI: 10.1021/acs.accounts.7b00161
Acc. Chem. Res. 2017, 50, 1808−1817

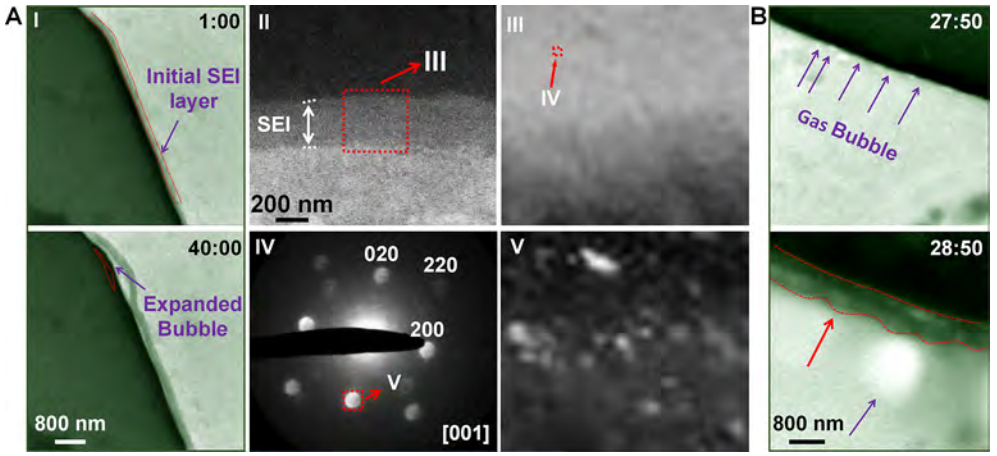

Figure 8. (A) I. Time series of TEM images showing the growth of a gas bubble emerging between the gold electrode and the SEI film. II. HAADF image of the SEI layer on a Ti electrode. The highlighted red dashed box indicates the nanobeam diffraction acquisition area. III. Reconstructed bright-field image obtained from the diffraction series. IV. Reconstructed virtual diffraction patterns selected from the region marked "IV" in panel III. V. Virtual dark-field image reconstructed using the selected single diffraction spot in panel IV. Adapted from (I) ref 48 and (II–V) ref 52. Copyright 2014 and 2015, respectively, American Chemical Society. (B) Gas bubble formation during lithiation of a Au electrode. Adapted from ref 48. Copyright 2014 American Chemical Society.

different Au–Li alloy phases have been identified through both ex situ and in situ studies,[60−63] the Au–Li reaction has never been observed directly. We studied the lithiation of a Au electrode in an electrochemical liquid cell using a commercial liquid electrolyte for lithium ion batteries.[64] Three distinct types of morphology changes were observed during the reaction, including gradual dissolution, explosive reaction, and local expansion/shrinkage. The local expansion/shrinkage of the Au electrode during lithiation induces cracks and is likely due to inhomogeneous lithiation reactions (Figure 7C). The explosive Li–Au reaction was attributed to adsorption and accumulation of the gaseous products on the electrode surface, which trigger the explosion of the Au electrode at a later stage (Figure 7D). As to the gradual dissolution, the Au electrode could react intensively with the electrolyte, resulting in stripping and dissolution of Au from the outer layer into the inner layer of the electrode (Figure 7E).

3.3. Electrolyte Decomposition: Solid Electrolyte Interphase and Bubble Formation

In general, the electrolyte solutions for Li batteries are composed of redox couples with the solvent as a reductant and the salt as an oxidant. The majority of species that are oxidized are solvent molecules, not the salt anions[65,66] The breakdown of a range of inorganic/salt complexes and reactions between complexes lead to the formation of a solid–electrolyte interphase (SEI).[67,68] The SEI layer protects the electrolytic solution and other battery components from undesirable reduction or oxidation. However, gas production during SEI formation on the active electrode can introduce defects and strain in the SEI film, thus leading to peeling of the SEI from the electrode.[48,52] There have been limited in situ studies on the direct observation and characterization of SEIs, largely because the SEI is air-sensitive and analyzing it in a battery cell is difficult. Zeng and co-workers achieved real-time observation of SEI formation using electrochemical liquid cell TEM.[48,64]

As shown in Figure 8A, the SEI film grows on the electrode as a result of the reduction of electrolyte corresponding to the electric sweeping (4 to 0 V). At the beginning, a thin SEI layer was observed on the Au electrode. Subsequently, a gap between the SEI film and the electrode was observed, and the emerged void between the SEI layer and active electrode promptly expanded, likely as a result of the released gas accompanied by the reactions of active electrode materials.

Further characterization of SEI confirmed the presence of C, O, and F elements. And, there were LiF nanocrystals (4–5 nm) distributed within the whole amorphous matrix layer.[52] Since it is hard to detect amorphous or small crystalline components, the presence of other inorganic components (e.g., Li_2CO_3, Li_2O) within the SEI cannot be excluded. It should be noted that gaseous products have been observed in many other electrochemical experiments. For example, bubbles can form from electrolyte decomposition induced PF_5 (Figure 8B). By replacement of Au with a Ti electrode, bubble formation can be significantly reduced, suggesting that Au may catalyze the bubble generation.[64]

4. ELECTRON BEAM EFFECTS

The electron beam effects on solid samples have been studied both theoretically and experimentally.[69] However, the effects of the electron beam during imaging of liquid samples can be different from those on solids, depending on the specific system and the role of various factors. Since several phenomena may occur simultaneously, such as solvated electrons, bond cleavage, and local heating, the radiation damage mechanisms is complicated.[7] When liquid cell TEM is used to study nanoparticle growth, the electron beam is often an energy source to trigger the reaction. The high-energy electron beam can induce decomposition of the liquid or precursor. Nanoparticle growth under the electron beam occurs above a certain dose threshold. However, with a sufficiently high dose, gaseous products, such as bubbles, can be generated in a solution, various radicals, including secondary electrons, can be generated and these species can further participate in the reactions.[70] To minimize the electron beam damage, one can consider reducing the accelerating voltage or lowering the electron dose. As all electron beam effects are dose-dependent, low-dose imaging can be an effective way to reduce electron beam damage in all systems. For electrochemical deposition using liquid cell TEM, beam effects are minimized at the reduced electron dose.[47,71,72] The observed dendritic growth or

DOI: 10.1021/acs.accounts.7b00161
Acc. Chem. Res. 2017, 50, 1808–1817

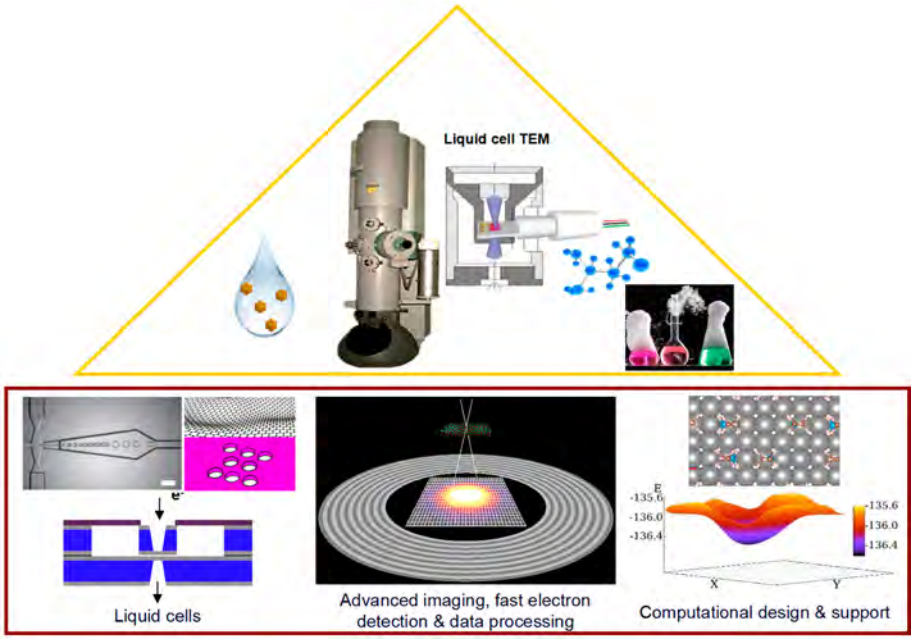

Figure 9. A powerful liquid cell TEM platform built upon liquid cell development, advanced imaging, fast electron detection, computational design, and data analysis (fluidic liquid cell drawing courtesy of Dr. Emory Chan; advanced imaging picture courtesy of Dr. Peter Ercius). The bottom right panel is reprinted with permission from ref 21. Copyright 2014 American Association for the Advancement of Science.

electrolyte decomposition were achieved only when an electric bias was applied in the electrochemical cell.[48,49,52]

5. FUTURE PERSPECTIVES

The ability to image through liquids with TEM has opened tremendous opportunities to study liquid-phase reactions and to reveal dynamic phenomena at solid–liquid interfaces in situ with high spatial and temporal resolution. In addition to visualization of colloidal nanocrystal growth and assembly and liquid-phase electrochemical reactions as discussed in this Account, there are many other applications of liquid environmental cell electron microscopy, such as imaging of soft or biological materials in liquid water, materials corrosion, and catalysis. Future advances in atomic-resolution liquid cell TEM would enable a significant leap in the study of dynamic processes of materials with high spatial and temporal resolution.

For the study of liquid-phase reactions or dynamic phenomena of materials at liquid–solid interfaces, we may also fully take advantage of aberration-corrected electron microscopes, advanced detectors, and other instrumentation development. As we know that TEM has advanced significantly with aberration-corrected optics, imaging with 0.5 Å spatial resolution[73] and EELS with 1 or 2 meV energy resolution[74] have been achieved. With the combination of advancement in EDS development, TEM is becoming more and more powerful in characterization of atomic structure, bonding, and chemical and structural properties of materials. In addition, with the development of advanced detectors,[21] high-speed data acquisition with 2.5 ms temporal resolution[21] has also been obtained. Other factors, such as optimization of the sample thickness, limiting electron beam damage, control of the sample environment, especially the liquid reaction or mixing, and quantitative measurements of reaction products, are also critical for revealing dynamic phenomena at liquid–solid interfaces with high resolution.

A new liquid cell platform (Figure 9) beyond the limits of current imaging capabilities is needed to achieve fast, atomic resolution TEM imaging through liquids. Such a platform will be built upon new liquid cell development, advanced imaging, fast electron detection, computational design, and data analysis. It will enable the controlled reactions in a liquid cell, advanced image acquisition with atomic resolution and at a fast speed, integrated analytical capabilities, comprehensive data processing and interpretation, thus the study of chemical reactions in solution will be revolutionized.

These efforts promote TEM as an analytical tool for chemical sciences in addition to materials science, physics and biology.

AUTHOR INFORMATION

Corresponding Author

*E-mail: hmzheng@lbl.gov.

ORCID

Haimei Zheng: 0000-0003-3813-4170

Notes

The authors declare no competing financial interest.

Biographies

Zhiyuan Zeng obtained his B.E. in Materials Physics from Central South University, China (2006) and his M.E. from the Department of Materials Science and Engineering of Zhejiang University, China (2008). He completed his Ph.D. in the School of Materials Science and Engineering of Nanyang Technological University, Singapore (2013). In February 2013, he started a Physicist Postdoctoral Fellowship in the Materials Sciences Division at Lawrence Berkeley National Laboratory under Dr. Haimei Zheng. His current research focuses on in situ multimodal characterization of Li/Na batteries and applications of two-dimensional nanosheets.

Wenjing Zheng obtained her B.S. in Chemical Engineering and Technology from Taizhou University, China (2010) and her M.S. in Material Engineering from Shijiazhuang Tiedao University, China

DOI: 10.1021/acs.accounts.7b00161
Acc. Chem. Res. 2017, 50, 1808–1817

(2014). She is currently a Ph.D. candidate at Tianjin University and a visiting student at Lawrence Berkeley National Laboratory. She is interested in nanoscale materials design, mechanisms, and catalysts.

Haimei Zheng earned her Ph.D. with Prof. Ramamoorthy Ramesh and Prof. Lourdes Salamanca-Riba at the University of Maryland, College Park (2004). She was a postdoc with Prof. Paul Alivisatos at the Department of Chemistry of the University of California, Berkeley, and jointly at the National Center for Electron Microscopy at Lawrence Berkeley National Laboratory. Currently she is a senior staff scientist in the Materials Sciences Division at Lawrence Berkeley National Laboratory and an adjunct professor in the Department of Materials Science and Engineering at the University of California, Berkeley. The primary research in her group is on physical and chemical processes of materials with a focus on liquid−solid interfaces, including nucleation, growth, and self-assembly of nanoparticles and electrolyte−electrode interfaces during electrochemical processes.

■ ACKNOWLEDGMENTS

We acknowledge the support from the U.S. Department of Energy, Office of Science, Office of Basic Energy Sciences, Materials Sciences and Engineering Division, under Contract DE-AC02-05-CH11231 within the KC22ZH Program.

■ REFERENCES

(1) Mirsaidov, U. M.; Zheng, H. M.; Casana, Y.; Matsudaira, P. Imaging protein structure in water at 2.7 nm resolution by transmission electron microscopy. *Biophys. J.* **2012**, *102*, L15−L17.
(2) Zheng, H.; Smith, R. K.; Jun, Y.-w.; Kisielowski, C.; Dahmen, U.; Alivisatos, A. P. Observation of single colloidal platinum nanocrystal growth trajectories. *Science* **2009**, *324*, 1309−1312.
(3) Ross, F. M. Opportunities and challenges in liquid cell electron microscopy. *Science* **2015**, *350*, aaa9886.
(4) Liao, H. G.; Zheng, H. M. Liquid cell transmission electron microscopy. *Annu. Rev. Phys. Chem.* **2016**, *67*, 719−747.
(5) Yoshida, H.; Kuwauchi, Y.; Jinschek, J. R.; Sun, K. J.; Tanaka, S.; Kohyama, M.; Shimada, S.; Haruta, M.; Takeda, S. Visualizing gas molecules interacting with supported nanoparticulate catalysts at reaction conditions. *Science* **2012**, *335*, 317−319.
(6) Zheng, H. M.; Meng, Y. S.; Zhu, Y. M. Frontiers of in situ electron microscopy. *MRS Bull.* **2015**, *40*, 12−18.
(7) de Jonge, N.; Ross, F. M. Electron microscopy of specimens in liquid. *Nat. Nanotechnol.* **2011**, *6*, 695−704.
(8) Williamson, M. J.; Tromp, R. M.; Vereecken, P. M.; Hull, R.; Ross, F. M. Dynamic microscopy of nanoscale cluster growth at the solid-liquid interface. *Nat. Mater.* **2003**, *2*, 532−536.
(9) Gai, P. L. Developments in in situ environmental cell high-resolution electron microscopy and applications to catalysis. *Top. Catal.* **2002**, *21*, 161−173.
(10) Liu, K.-L.; Wu, C.-C.; Huang, Y.-J.; Peng, H.-L.; Chang, H.-Y.; Chang, P.; Hsu, L.; Yew, T.-R. Novel microchip for in situ TEM imaging of living organisms and bio-reactions in aqueous conditions. *Lab Chip* **2008**, *8*, 1915−1921.
(11) Jonge, N. d.; Peckys, D. B.; Kremers, G. J.; Piston, D. W. Electron microscopy of whole cells in liquid with nanometer resolution. *Proc. Natl. Acad. Sci. U. S. A.* **2009**, *106*, 2159−2164.
(12) Yin, Y.; Alivisatos, A. P. Colloidal nanocrystal synthesis and the organic-inorganic interface. *Nature* **2005**, *437*, 664−670.
(13) Banfield, J. F.; Welch, S. A.; Zhang, H.; Ebert, T. T.; Penn, R. L. Aggregation-based crystal growth and microstructure development in natural iron oxyhydroxide biomineralization products. *Science* **2000**, *289*, 751−754.
(14) Pacholski, C.; Kornowski, A.; Weller, H. Self-assembly of ZnO: from nanodots to nanorods. *Angew. Chem., Int. Ed.* **2002**, *41*, 1188−1191.
(15) Watzky, M. A.; Finney, E. E.; Finke, R. G. Transition-metal nanocluster size vs formation time and the catalytically effective nucleus number: a mechanism-based treatment. *J. Am. Chem. Soc.* **2008**, *130*, 11959−11969.
(16) Liao, H.-G.; Cui, L.; Whitelam, S.; Zheng, H. Real-time imaging of Pt_3Fe nanorod growth in solution. *Science* **2012**, *336*, 1011−1014.
(17) Powers, A. S.; Liao, H.-G.; Raja, S. N.; Bronstein, N. D.; Alivisatos, A. P.; Zheng, H. Tracking nanoparticle diffusion and interaction during self-assembly in a liquid cell. *Nano Lett.* **2017**, *17*, 15−20.
(18) Xin, H. L. L.; Zheng, H. M. In situ observation of oscillatory growth of bismuth nanoparticles. *Nano Lett.* **2012**, *12*, 1470−1474.
(19) Yuk, J. M.; Park, J.; Ercius, P.; Kim, K.; Hellebusch, D. J.; Crommie, M. F.; Lee, J. Y.; Zettl, A.; Alivisatos, A. P. High-resolution EM of colloidal nanocrystal growth using graphene liquid cells. *Science* **2012**, *336*, 61−64.
(20) Borodko, Y.; Ercius, P.; Zherebetskyy, D.; Wang, Y.; Sun, Y.; Somorjai, G. From single atoms to nanocrystals: photoreduction of $[PtCl_6]^{2-}$ in aqueous and tetrahydrofuran solutions of PVP. *J. Phys. Chem. C* **2013**, *117*, 26667−26674.
(21) Liao, H.-G.; Zherebetskyy, D.; Xin, H.; Czarnik, C.; Ercius, P.; Elmlund, H.; Pan, M.; Wang, L.-W.; Zheng, H. Facet development during platinum nanocube growth. *Science* **2014**, *345*, 916−919.
(22) Manna, L.; Scher, E. C.; Alivisatos, A. P. Synthesis of soluble and processable rod-, arrow-, teardrop-, and tetrapod-shaped CdSe nanocrystals. *J. Am. Chem. Soc.* **2000**, *122*, 12700−12706.
(23) Schliehe, C.; Juarez, B. H.; Pelletier, M.; Jander, S.; Greshnykh, D.; Nagel, M.; Meyer, A.; Foerster, S.; Kornowski, A.; Klinke, C.; Weller, H. Ultrathin PbS sheets by two-dimensional oriented attachment. *Science* **2010**, *329*, 550−553.
(24) Cho, K.-S.; Talapin, D. V.; Gaschler, W.; Murray, C. B. Designing PbSe nanowires and nanorings through oriented attachment of nanoparticles. *J. Am. Chem. Soc.* **2005**, *127*, 7140−7147.
(25) Liao, H.-G.; Zheng, H. Liquid cell transmission electron microscopy study of platinum iron nanocrystal growth and shape evolution. *J. Am. Chem. Soc.* **2013**, *135*, 5038−5043.
(26) Min, Y.; Akbulut, M.; Kristiansen, K.; Golan, Y.; Israelachvili, J. The role of interparticle and external forces in nanoparticle assembly. *Nat. Mater.* **2008**, *7*, 527−538.
(27) Yusuf, H.; Kim, W.-G.; Lee, D. H.; Guo, Y.; Moffitt, M. G. Size control of mesoscale aqueous assemblies of quantum dots and block copolymers. *Langmuir* **2007**, *23*, 868−878.
(28) Kumar, C. S. S. R.; Mohammad, F. Magnetic nanomaterials for hyperthermia-based therapy and controlled drug delivery. *Adv. Drug Delivery Rev.* **2011**, *63*, 789−808.
(29) Polshettiwar, V.; Luque, R.; Fihri, A.; Zhu, H.; Bouhrara, M.; Basset, J.-M. Magnetically recoverable nanocatalysts. *Chem. Rev.* **2011**, *111*, 3036−3075.
(30) Frey, N. A.; Peng, S.; Cheng, K.; Sun, S. Magnetic nanoparticles: synthesis, functionalization, and applications in bioimaging and magnetic energy storage. *Chem. Soc. Rev.* **2009**, *38*, 2532−2542.
(31) Woehl, T. J.; Jungjohann, K. L.; Evans, J. E.; Arslan, I.; Ristenpart, W. D.; Browning, N. D. Experimental procedures to mitigate electron beam induced artifacts during in situ fluid imaging of nanomaterials. *Ultramicroscopy* **2013**, *127*, 53−63.
(32) Woehl, T. J.; Evans, J. E.; Arslan, I.; Ristenpart, W. D.; Browning, N. D. Direct in situ determination of the mechanisms controlling nanoparticle nucleation and growth. *ACS Nano* **2012**, *6*, 8599−8610.
(33) Liang, W.-I.; Zhang, X.; Bustillo, K.; Chiu, C.-H.; Wu, W.-W.; Xu, J.; Chu, Y.-H.; Zheng, H. In situ study of spinel ferrite nanocrystal growth using liquid cell transmission electron microscopy. *Chem. Mater.* **2015**, *27*, 8146−8152.
(34) Liang, W.-I.; Zhang, X.; Zan, Y.; Pan, M.; Czarnik, C.; Bustillo, K.; Xu, J.; Chu, Y.-H.; Zheng, H. In situ study of Fe_3Pt−Fe_2O_3 core−shell nanoparticle formation. *J. Am. Chem. Soc.* **2015**, *137*, 14850−14853.
(35) Beck, W.; Souza, C. G. S.; Silva, T. L.; Jafelicci, M.; Varanda, L. C. Formation mechanism via a heterocoagulation approach of FePt nanoparticles using the modified polyol process. *J. Phys. Chem. C* **2011**, *115*, 10475−10482.

DOI: 10.1021/acs.accounts.7b00161
Acc. Chem. Res. 2017, 50, 1808−1817

(36) Shukla, N.; Liu, C.; Jones, P. M.; Weller, D. FTIR study of surfactant bonding to FePt nanoparticles. *J. Magn. Magn. Mater.* **2003**, *266*, 178−184.
(37) Ye, X. C.; Jones, M. R.; Frechette, L. B.; Chen, Q.; Powers, A. S.; Ercius, P.; Dunn, G.; Rotskoff, G. M.; Nguyen, S. C.; Adiga, V. P.; Zettl, A.; Rabani, E.; Geissler, P. L.; Alivisatos, A. P. Single-particle mapping of nonequilibrium nanocrystal transformations. *Science* **2016**, *354*, 874−877.
(38) Schneider, N. M.; Norton, M. M.; Mendel, B. J.; Grogan, J. M.; Ross, F. M.; Bau, H. H. Electron-water interactions and implications for liquid cell electron microscopy. *J. Phys. Chem. C* **2014**, *118*, 22373−22382.
(39) Ahn, T. Y.; Hong, S. P.; Kim, S. I.; Kim, Y. W. In situ liquid-cell transmission electron microscopy for direct observation of concentration-dependent growth and dissolution of silver nanoparticles. *RSC Adv.* **2015**, *5*, 82342−82345.
(40) Jiang, Y. Y.; Zhu, G. M.; Dong, G. X.; Lin, F.; Zhang, H.; Yuan, J.; Zhang, Z.; Jin, C. H. Probing the oxidative etching induced dissolution of palladium nanocrystals in solution by liquid cell transmission electron microscopy. *Micron* **2017**, *97*, 22−28.
(41) Jiang, Y. Y.; Zhu, G. M.; Lin, F.; Zhang, H.; Jin, C. H.; Yuan, J.; Yang, D. R.; Zhang, Z. In situ study of oxidative etching of palladium nanocrystals by liquid cell electron microscopy. *Nano Lett.* **2014**, *14*, 3761−3765.
(42) Tiller, W. A. Dendrites - Understanding of this familiar phenomenon has led to the development of useful man-made materials. *Science* **1964**, *146*, 871−879.
(43) Langer, J. S. Dendrites, viscous fingers, and the theory of pattern formation. *Science* **1989**, *243*, 1150−1156.
(44) Miyata, Y.; Glicksman, M. E.; Tirmizi, S. H. Dendritic growth with interfacial energy anisotropy. *J. Cryst. Growth* **1991**, *110*, 683−691.
(45) Libbrecht, K. G.; Tanusheva, V. M. Electrically induced morphological instabilities in free dendrite growth. *Phys. Rev. Lett.* **1998**, *81*, 176−179.
(46) Börzsönyi, T.; Tóth-Katona, T.; Buka, Á.; Gránásy, L. Dendrites regularized by spatially homogeneous time-periodic forcing. *Phys. Rev. Lett.* **1999**, *83*, 2853−2856.
(47) Radisic, A.; Vereecken, P. M.; Hannon, J. B.; Searson, P. C.; Ross, F. M. Quantifying electrochemical nucleation and growth of nanoscale clusters using real-time kinetic data. *Nano Lett.* **2006**, *6*, 238−242.
(48) Zeng, Z. Y.; Liang, W. I.; Liao, H. G.; Xin, H. L. L.; Chu, Y. H.; Zheng, H. M. Visualization of electrode-electrolyte interfaces in $LiPF_6$/EC/DEC electrolyte for lithium ion batteries via in Situ TEM. *Nano Lett.* **2014**, *14*, 1745−1750.
(49) Sun, M.; Liao, H.-G.; Niu, K.; Zheng, H. Structural and morphological evolution of lead dendrites during electrochemical migration. *Sci. Rep.* **2013**, *3*, 3227.
(50) Chen, X.; Noh, K. W.; Wen, J. G.; Dillon, S. J. In situ electrochemical wet cell transmission electron microscopy characterization of solid-liquid interactions between Ni and aqueous $NiCl_2$. *Acta Mater.* **2012**, *60*, 192−198.
(51) White, E. R.; Singer, S. B.; Augustyn, V.; Hubbard, W. A.; Mecklenburg, M.; Dunn, B.; Regan, B. C. In situ transmission electron microscopy of lead dendrites and lead ions in aqueous solution. *ACS Nano* **2012**, *6*, 6308−6317.
(52) Zeng, Z.; Zhang, X.; Bustillo, K.; Niu, K.; Gammer, C.; Xu, J.; Zheng, H. In situ study of lithiation and delithiation of MoS_2 nanosheets using electrochemical liquid cell transmission electron microscopy. *Nano Lett.* **2015**, *15*, 5214−5220.
(53) Gu, M.; Parent, L. R.; Mehdi, B. L.; Unocic, R. R.; McDowell, M. T.; Sacci, R. L.; Xu, W.; Connell, J. G.; Xu, P.; Abellan, P.; Chen, X.; Zhang, Y.; Perea, D. E.; Evans, J. E.; Lauhon, L. J.; Zhang, J.-G.; Liu, J.; Browning, N. D.; Cui, Y.; Arslan, I.; Wang, C.-M. Demonstration of an electrochemical liquid cell for operando transmission electron microscopy observation of the lithiation/delithiation behavior of Si nanowire battery anodes. *Nano Lett.* **2013**, *13*, 6106−6112.
(54) Holtz, M. E.; Yu, Y.; Gunceler, D.; Gao, J.; Sundararaman, R.; Schwarz, K. A.; Arias, T. A.; Abruña, H. D.; Muller, D. A. Nanoscale imaging of lithium ion distribution during in situ operation of battery electrode and electrolyte. *Nano Lett.* **2014**, *14*, 1453−1459.
(55) Abellan, P.; Mehdi, B. L.; Parent, L. R.; Gu, M.; Park, C.; Xu, W.; Zhang, Y.; Arslan, I.; Zhang, J.-G.; Wang, C.-M.; Evans, J. E.; Browning, N. D. Probing the degradation mechanisms in electrolyte solutions for Li-ion batteries by in situ transmission electron microscopy. *Nano Lett.* **2014**, *14*, 1293−1299.
(56) Yuk, J. M.; Seo, H. K.; Choi, J. W.; Lee, J. Y. Anisotropic lithiation onset in silicon nanoparticle anode revealed by in situ graphene liquid cell electron microscopy. *ACS Nano* **2014**, *8*, 7478−7485.
(57) Gu, L.; Zhu, C. B.; Li, H.; Yu, Y.; Li, C. L.; Tsukimoto, S.; Maier, J.; Ikuhara, Y. Direct observation of lithium staging in partially delithiated $LiFePO_4$ at atomic resolution. *J. Am. Chem. Soc.* **2011**, *133*, 4661−4663.
(58) Niu, J.; Kushima, A.; Qian, X.; Qi, L.; Xiang, K.; Chiang, Y.-M.; Li, J. In situ observation of random solid solution zone in $LiFePO_4$ electrode. *Nano Lett.* **2014**, *14*, 4005−4010.
(59) Xiao, J.; Wang, X.; Yang, X.-Q.; Xun, S.; Liu, G.; Koech, P. K.; Liu, J.; Lemmon, J. P. Electrochemically induced high capacity displacement reaction of PEO/MoS_2/Graphene nanocomposites with lithium. *Adv. Funct. Mater.* **2011**, *21*, 2840−2846.
(60) Lee, Y. J.; Lee, Y.; Oh, D.; Chen, T.; Ceder, G.; Belcher, A. M. Biologically activated noble metal alloys at the nanoscale: For lithium ion battery anodes. *Nano Lett.* **2010**, *10*, 2433−2440.
(61) Taillades, G.; Benjelloun, N.; Sarradin, J.; Ribes, M. Metal-based very thin film anodes for lithium ion microbatteries. *Solid State Ionics* **2002**, *152-153*, 119−124.
(62) Yuan, L.; Liu, H. K.; Maaroof, A.; Konstantinov, K.; Liu, J.; Cortie, M. Mesoporous gold as anode material for lithium-ion cells. *J. New Mater. Electrochem. Syst.* **2007**, *10*, 95−99.
(63) Laik, B.; Eude, L.; Pereira-Ramos, J. P.; Cojocaru, C. S.; Pribat, D.; Rouviere, E. Silicon nanowires as negative electrode for lithium-ion microbatteries. *Electrochim. Acta* **2008**, *53*, 5528−5532.
(64) Zeng, Z.; Liang, W.-I.; Chu, Y.-H.; Zheng, H. In situ TEM study of the Li-Au reaction in an electrochemical liquid cell. *Faraday Discuss.* **2014**, *176*, 95−107.
(65) Moshkovich, M.; Gofer, Y.; Aurbach, D. Investigation of the electrochemical windows of aprotic alkali metal (Li,Na,K) salt solutions. *J. Electrochem. Soc.* **2001**, *148*, E155−E167.
(66) Aurbach, D.; Talyosef, Y.; Markovsky, B.; Markevich, E.; Zinigrad, E.; Asraf, L.; Gnanaraj, J. S.; Kim, H.-J. Design of electrolyte solutions for Li and Li-ion batteries: a review. *Electrochim. Acta* **2004**, *50*, 247−254.
(67) Unocic, R. R.; Sun, X.-G.; Sacci, R. L.; Adamczyk, L. A.; Alsem, D. H.; Dai, S.; Dudney, N. J.; More, K. L. Direct visualization of solid electrolyte interphase formation in lithium-ion batteries with in situ electrochemical transmission electron microscopy. *Microsc. Microanal.* **2014**, *20*, 1029−1037.
(68) Sacci, R. L.; Dudney, N. J.; More, K. L.; Parent, L. R.; Arslan, I.; Browning, N. D.; Unocic, R. R. Direct visualization of initial SEI morphology and growth kinetics during lithium deposition by in situ electrochemical transmission electron microscopy. *Chem. Commun.* **2014**, *50*, 2104−2107.
(69) Egerton, R. F.; Li, P.; Malac, M. Radiation damage in the TEM and SEM. *Micron* **2004**, *35*, 399−409.
(70) Grogan, J. M.; Schneider, N. M.; Ross, F. M.; Bau, H. H. Bubble and pattern formation in liquid induced by an electron beam. *Nano Lett.* **2014**, *14*, 359−364.
(71) Radisic, A.; Ross, F. M.; Searson, P. C. In situ study of the growth kinetics of individual island electrodeposition of copper. *J. Phys. Chem. B* **2006**, *110*, 7862−7868.
(72) den Heijer, M.; Shao, I.; Radisic, A.; Reuter, M. C.; Ross, F. M. Patterned electrochemical deposition of copper using an electron beam. *APL Mater.* **2014**, *2*, 022101.
(73) Rossell, M.; Watanabe, M.; Erni, R.; Radmilovic, V.; Dahmen, U. Quantitative Li mapping in Al alloys by sub-eV resolution energy-

DOI: 10.1021/acs.accounts.7b00161
Acc. Chem. Res. 2017, 50, 1808−1817

filtering transmission electron microscopy (EFTEM) in the aberration-corrected, monochromated TEAM 0.5 instrument. *Microsc. Microanal.* **2009**, *15*, 430−431.
(74) Michel, E.; Ibach, H.; Schneider, C. M. High resolution electron energy loss spectroscopy of spin waves in ultra-thin cobalt films. *Surf. Interface Anal.* **2016**, *48*, 1104−1107.

DOI: 10.1021/acs.accounts.7b00161
Acc. Chem. Res. 2017, 50, 1808−1817